Biosensors and Bioelectronics 49 (2013) 184–191

Contents lists available at SciVerse ScienceDirect

Biosensors and Bioelectronics

journal homepage: www.elsevier.com/locate/bios

Facile synthesis of hierarchically aloe-like gold micro/nanostructures for ultrasensitive DNA recognition

Lei Shi [a], Zhenyu Chu [a], Yu Liu [a], Wanqin Jin [a,*], Xiaojun Chen [b]

[a] State Key Laboratory of Materials-Oriented Chemical Engineering, College of Chemistry and Chemical Engineering, Nanjing University of Technology, Nanjing 210009, PR China
[b] College of Sciences, Nanjing University of Technology, Nanjing 210009, PR China

ARTICLE INFO

Article history:
Received 10 February 2013
Received in revised form
24 April 2013
Accepted 6 May 2013
Available online 14 May 2013

Keywords:
Hierarchical gold micro/nanostructures
Hydrophilicity
Gold electro-deposition kinetics
Electrochemical DNA biosensor

ABSTRACT

Well-defined hierarchically aloe-like gold micro/nanostructures (HAG) are one-step electrochemically fabricated without introducing any template or surfactant. The formation kinetics of the HAG can be described as a nucleation and three-dimensional growth process controlled by the reactant diffusion from the solution side. As the applied electro-deposition potential moved in the negative direction, the gold crystal density increased, and the crystal shape changed from a quasi-spherical to dendritic fractal morphology. Under the optimal potential of −0.1 V and the time of 10 min, well-defined HAG possessing a hydrophilic surface with large effective area (ca. 8 times of its geometrical area) were obtained, which was used as the substrate for fabricating an ultrasensitive DNA biosensor. The DNA biosensor displayed a significantly enhanced detection limit of 12 aM, a wide linear response from 50 aM to 1 pM, as well as good selectivity, stability and reusability. This efficient DNA molecule immobilization platform may have implications in the preparation of many other gold micro/nanostructures (GMNs) with interesting properties and application potentials in many fields, such as biosensing, biocatalysis and biofuel cells.

1. Introduction

The development of novel DNA biosensors for highly sensitive and selective detection is of critical importance in many aspects, including analysis of gene sequencing which has been critical in the identification of the genetic risk factors, medical diagnostics, food safety screening, and environmental monitoring (Sassolas et al., 2008; Liu et al., 2009). Consequently, a wide variety of DNA biosensors have been developed, which are mainly based on three detection strategies of electrical (Gao et al., 2011; Soleymani et al., 2007), optical (Zhang et al., 2005) and piezoelectric transduction techniques (Patolsky et al., 2003). Considering the advantages of the simplicity, cheapness, portability, and especially easy of miniaturization, which would be employed to produce microchip based DNA bioassays, the electrochemical methods have become one of the most attractive techniques for DNA biosensors (Drummond et al., 2003).

The developments in the field of nanomaterials create promising opportunities to design and construct novel electrochemical detection processes, which have been widely used to enhance the sensitivity in DNA detections. Gold micro/nanostructures (GMNs), some of the most extensively studied nanomaterials, are considered as pivotal materials and building blocks in the nanoelectronics, biology and material science (Daniel and Astruc, 2004; Giljohann et al., 2010; Zhang et al., 2012). Owing to the unique physical and chemical properties, GMNs have become excellent scaffolds in the fabrication of chemical and biological sensors (Sun and Xia, 2004; Chen et al., 2008; Wang et al., 2005; Lapierre-Devlin et al., 2005). Firstly, they could provide high surface-to-volume ratio with excellent biocompatibility. Secondly, the properties of GMNs can be readily tuned by varying their size, morphology and surrounding chemical environment. Thirdly, GMNs could offer a multi-functional platform with a wide range of organic or biological ligands for selective binding (Saha et al., 2012). All these properties make GMNs the proper candidates for constructing novel sensing strategies with improved sensitivity, stability and selectivity. For example, gold nanowires prepared by Kelley group were served as a nanoelectrode platform for DNA sensing with detection limit of approximately 0.1 pM (Lapierre-Devlin et al., 2005). Hu et al. (2008) prepared a nanoporous gold electrode, and based on which, an electrochemical ultrasensitive DNA biosensor was developed with the detection limit of 28 aM. In addition, Jagerszki et al. (2007) fabricated a gold nanotubes modified electrode, which was served for label-free DNA assay, showing a detection limit of 0.1 nM. Furthermore, Andreu et al. (2006) presented a DNA biosensor on a gold array, in which they addressed the problems on the miniaturization of the electrode system and the increase of surface area. The introduction of GMNs into the DNA biosensors efficiently

* Corresponding author. Tel.: +86 25 8317 2266; fax: +86 25 8317 2292.
E-mail address: wqjin@njut.edu.cn (W. Jin).

0956-5663/$ - see front matter © 2013 Elsevier B.V. All rights reserved.
http://dx.doi.org/10.1016/j.bios.2013.05.012

increased the specific biosensing surface and further more probe molecules could be immobilized, which imparted them obviously excellent properties and performances. However, some drawbacks might exist during the synthesis process of GMNs that the templates were usually used, because the preparation of templates is complicated and the additional removal of templates might destroy the as-prepared GMNs.

Thus, the construction of GMNs by a facile approach for fabricating a high-performance electrochemical DNA biosensor is challenging. Recently, L. Wang et al. (2011) prepared a nanoflower-like GMNs electrode by a simple one-step electrodeposition method in pH 5.0 $HAuCl_4$ solution. A DNA biosensor was fabricated based on this modified electrode with a detection limit of 1 pM. Li and his coworkers prepared dendritic gold nanostructure (DenG) through direct electrodeposition under −1.5 V using the hydrogen bubble evolved during the process as a dynamic template. They also fabricated a DNA biosensor to distinguish the DNA strands with a sensitivity of 1 fM (Li et al., 2011). Jiao's group successfully fabricated homogeneously dispersed and hierarchical flower-like gold microspheres (HHFG) by adopting a three-step electrodeposition. The morphology of HHFG could be regulated through altering the current density and the time of each step. They constructed a DNA sensor for detecting cauliflower mosaic virus gene segment with a detection limit of 19 fM (X.X. Wang et al., 2011). The development of GMNs by simple electrodeposition method is very attractive for the applications in DNA biosensors. However, the role of nanostructuring in modulating bio-detection sensitivity has been less addressed and needs further exploration in detail.

Herein, the electro-formation of GMNs on ITO electrodes in the nanometer scale range was investigated. In the potential range covered from 0.3 V to −0.3 V, the aggregate of GMNs is controlled by a nucleation and growth process under diffusion limit of $AuCl_4^-$ ions from the solution side. Along with negative shift of the applied potential and extension of the deposition time, the shape of GMNs changed from Euclidean to dendritic fractal patterns, and the density of GMNs became enhanced as well. At the optimal potential of −0.1 V and time of 10 minutes, well-defined HAG was fabricated, possessing eminent hydrophilicity and large effective area, characterized by contact angle measurement and cyclic voltammetric (CV) technique, respectively. An ultrasensitive DNA biosensor was designed based on the HAG, achieving a detection limit of 12 aM and a wide linear response ranging from 50 aM to 1 pM. The proposed HAG is highly recommended as an improved biosensing platform for biomolecule immobilizations and bioassays.

2. Experimental section

2.1. Chemicals and materials

All of the chemicals used were of reagent grade or better. Gold nanoparticles (GNPs) with 10 nm diameter were purchased from Strem Chemicals, Gold(III) chloride trihydrate ($HAuCl_4$, 99.99%) was obtained from Alfa Aesar, 6-Mercapto-1-hexanol (MCH, 97%) and methylene blue (MB) were purchased from Sigma Aldrich. $HClO_4$, $K_3Fe(CN)_6$, NaOH, C_2H_5OH, $(CH_3)_2CO$, NaCl, NaH_2PO_4 and Na_2HPO_4 were brought from Sinopharm Chemical Reagent Co., Ltd. The commercial glass slides coated with a layer of 50 nm indium-tin oxide (ITO) with resistance of 50 $\Omega\,sq^{-1}$ were used as conductive substrates. Water (18.2 MΩ•cm) was obtained from an ultrafilter system (Milli-Q, Millipore, MA). Oligonucleotides were purchased from shanghai sangon. DNA capture probe (cDNA): 5′-HS-$(CH_2)_6$-GTT CTT CTC ATC ATC GAC-3′, DNA target (tDNA): 3′-CAA GAA GAG TAG TAG CTG TTTTTT GTC GAC CCT GCG CCA CGC-5′, report probe (rDNA): 5′-CAG CTG GGA CGC GGT GCG-$(CH_2)_6$-HS-3′, one base mismatched tDNA: 3′-CAA GAA GAC TAG TAG CTG TTTTTT GTC GAC CCT GCG CCA CGC-5′, full mismatched tDNA: 3′-ACC TAC CTA GCT ATC TTC TTTTTT GTC GAC CCT GCG CCA CGC-5′. DNA immobilization buffer: 10 mM Tris–HCl, 1 mM EDTA, 10 mM TCEP, and 0.1 M NaCl (pH 7.4). Hybridization buffer: 10 mM phosphate buffered saline (PBS, pH 7.4) with 0.25 M NaCl.

2.2. Fabrication of GMNs through the electrochemical deposition

In the experiment, ITO (geometric area = 0.12 cm^2) was used as the working electrode, which was ultrasonic cleaned sequentially for 10 min each in acetone, 10% NaOH in ethanol, and distilled water. The chronoamperometric method was employed for the electrochemical deposition, in which the deposition potential and time were adjusted to obtain GMNs with various morphologies. Different deposition potentials (0.3 V, 0.1 V, −0.1 V or −0.3 V) and deposition time (from 2 to 15 min) were adopted, respectively. For the typical synthesis of HAG, the electrolyte containing 12 mM of $HAuCl_4$ and 0.05 M of $HClO_4$ was prepared with reagent-grade chemicals and distilled water, and the potential of −0.1 V and deposition time of 10 min were applied.

2.3. Materials characterization

The morphologies of the as-prepared GMNs were observed by field-emission scanning electron microscopy (FESEM, Hitachi S4800), and the chemical composition of HAG was determined by energy-dispersive X-ray spectroscopy (EDX, Hitachi S4800). Analysis of the X-ray photoelectron spectra (XPS) was performed on an ESCLAB MKII. Contact angles were measured on a drop shape analysis system G10/DSA10 contact angle system, and a 5 μL water droplet was dropped on the surface of various GMNs electrodes.

2.4. Immobilization and hybridization of DNA molecules

The GMNs electrodes were incubated in the immobilization solution containing 5 μM of thiolated cDNA at room temperature for 5 h. After unbound cDNA was washed away with distilled water, the unreacted active surface groups were subsequently passivated by reaction with 500 nM MCH solution for 2 h.

The rDNA–GNP conjugates were prepared with the following procedure (Zhang et al., 2007). The GNPs were firstly added to the thiolated rDNA in sterilized water and incubated at 4 °C for 16 h. Then rDNA–GNPs conjugates were aged by gradually addition of 2 M NaCl every 30 min to reach a final salt concentration of 0.1 M NaCl. The mixed solution was incubated for 48 h and finally the solution was centrifuged for 30 min at 4 °C with the supernatant being removed. The red oily precipitate was washed with 10 mM PBS, recentrifuged, and then redispersed in 10 mM PBS buffer. Add the tDNA in series concentrations to the rDNA–GNP conjugates in centrifuge tubes and incubate the solution for 1 h at 37 °C.

The cDNA attached HAG electrodes were immersed in the hybridization buffer containing a series concentration of tDNA for 2 h, which were then immersed into 1 mM MB in PBS for 30 min, followed by thoroughly rinsing with PBS.

2.5. Electrochemical measurements

All electrochemical experiments were performed with a CHI 660C electrochemical workstation (Shanghai Chenhua, China). A conventional three-electrode configuration was employed during the experiment, which involved a HAG working electrode, a platinum auxiliary electrode, and an Ag/AgCl (saturated KCl) reference electrode. All potentials herein are referenced to the Ag/AgCl.

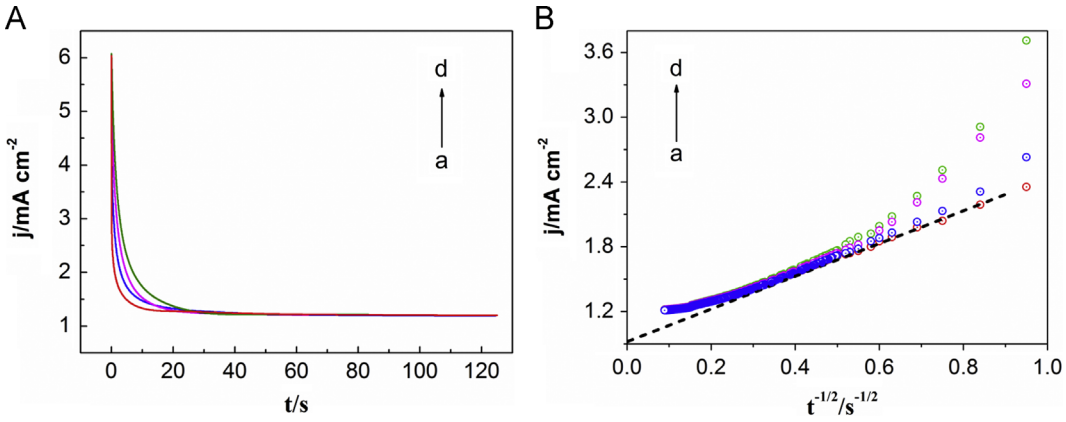

Fig. 1. (A) Current density (j) vs. time (t) curves (B) j vs. $t^{-1/2}$ curves for the gold micro/nanostructures electrodeposition at different potentials of (a) −0.3 V, (b) −0.1 V, (c) 0.1 V and (d) 0.3 V.

3. Results and discussion

3.1. Optimization of HAG electrodes

It was shown that a chronoamperometric method is a powerful tool for studying the nucleation and crystal growth mechanism during the initial stages of metal electrocrystallization. Under different potentiostatic conditions from −0.3 V to 0.3 V, all the current transients almost exhibited continuous current decay, which was related to the double-layer charging process (Cao et al., 2001; Depestel and Strubbe, 2004). Finally, steady current values were reached, owing to a steady free-convective diffusion process (Fig. 1A). The current density (j) showed linear relationship with $t^{-1/2}$ over a relatively large range of time (t), confirming that a nucleation and 3d growth process under diffusion control took place (Fig. 1B) (Finot et al., 1999; Mazaira et al., 2009; Ivanova and Zamborini, 2010).

From the j value and the $HAuCl_4$ concentration, $c_i = 1.2 \times 10^{-5}$ mol/cm^3, the value of the diffusion coefficient (D_i) of $HAuCl_4$ in the solution was estimated from the Eq. (1) (Martin et al., 1997).

$$j = zFD_i c_i/\delta \quad (1)$$

where z is the number of electrons transferred, F is Faraday's constant, and δ is the thickness of the diffusion layer. By taking for the quiescent solution the value $\delta = 0.025$ cm and $z = 3$, it results in $D_i = 8.6 \times 10^{-6}$ cm^2/s, in agreement with values of D_i reported in the literature ($D_i \approx 10^{-5}$ cm^2/s) for the diffusion of complex metal ion in aqueous solutions.

FESEM characterizations of GMNs deposited under different deposition potentials were carried out, as shown in Fig. 2. For a constant electrodeposition charge of 0.2 C, as the potential shifted from 0.3 V to −0.3 V, the crystal density increased due to the faster nucleation rate on the oversaturation at higher overpotentials (Fig. 2A, C, E and G). In addition, the trend to produce dendritic-type morphologies also increased (Fig. 2B, D, F and H). Since the overall electrochemical process was under mass transport kinetic control from the solution side, the evolution from a quasi-spherical shape to a dendritic pattern should be attributed to the influence of potentials. As the applied potential was set as 0.3 V, the growing aggregate tended to develop a faceted and kinked surface even with some unstable branches and maintain its original rounded shape for an isotropic barrier was considered (Smilauer and Vvedenski, 1995; Jacobsen et al., 1995). When the applied potential moved in the negative direction ($E = 0.1$ V, −0.1V and −0.3 V), the gold adatoms formed by discharge on gold coupled with a stronger anisotropic energy barrier at gold crystal step edges. More and more arms and branches were observed and either a starlike or a dendritic-like shape was obtained (Brune et al., 1996).

The GMNs electrodes were also electrochemically characterized in a 10 mM $K_3Fe(CN)_6$ containing 3 M KCl solution at a scan rate of 100 mV s^{-1}. The applied potential ranging from 0.3 V to −0.3 V was related to the existence of increased peak currents and decreased peak-to-peak separation (Supplementary materials, Fig. S1A). The effective electrochemical surface area of the GMNs electrode was estimated from the Randles–Sevcik equation (Xiao et al., 2008; Song et al., 2011). Since the effective surface area is proportional to $i_p/v^{1/2}$, CVs of these electrodes were measured at a variety of scan rates (Supplementary materials, Fig. S1B). Along with the deposition potential moved from 0.3 V to −0.3 V, the effective surface area of these GMNs electrodes were determined to be 0.29, 0.43, 0.94 and 0.97 cm^2, whereas the geometrical area of the bare ITO electrode was only 0.12 cm^2, therefore roughness factor (R_f) were calculated to be 2.4, 3.6, 7.8 and 8.1, respectively. It is obvious that a larger active surface area would be obtained under a more negative deposition potential.

Since the aim of this work is fabricating a highly sensitive DNA biosensor based on the GMNs electrode, characteristics of the surface should be taken into a close consideration. Homogeneity of chemical and physical structure, surface architecture, surface tension, hydrophobicity and hydrophilicity, and control of spacing between the probes are among the representative parameters influencing the performance of biosensors. Among various issues required further study, we believe reducing steric hindrance on the surface is an outstanding target. Steric hindrance, between the solid surface and target biomolecules as well as among the immobilized capture biomolecules, strongly hampers biomolecular interactions on the surface. Therefore, both fabrication of surface providing immobilized biomolecules with the environment like the solution phase and immobilization strategy holding biomolecules in a specific manner are essential for success of the biosensor fabrication. First of all, a hydrophilic surface with moderate wettability is required, since a hydrophobic surface might induce strongly irreversible adsorption and denature the protein's native confirmation and bioactivity (Ma et al., 2007). Thus, contact angle (θ) measurements of these GMNs modified ITO were investigated, as shown in the insets of Fig. 2. When the potential changed from 0.3 V to −0.1 V, slight decrease of θ values from 59.2° to 52.2° was observed, showing improved hydrophilicity. However, as the deposition potential moved to −0.3 V, the θ value increased significantly to be 110.2°, showing the obvious hydrophobicity. At the moment, a higher density of GMNs might cause the individual gold particle link with each other, resulting in a more rough and porous surface.

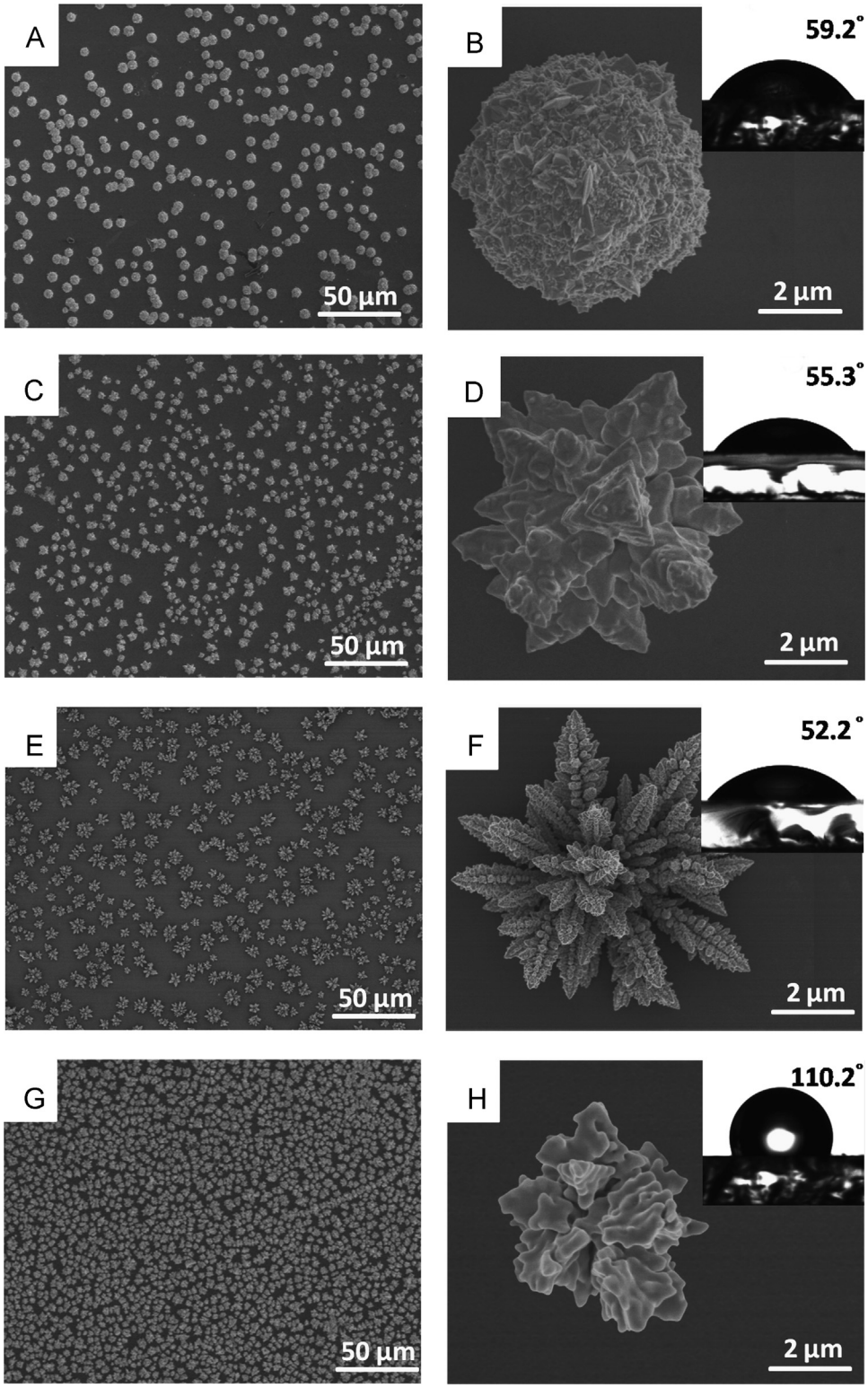

Fig. 2. FESEM images of different GMNs electrodeposited on the ITO substrates at (A) 0.3 V, (C) 0.1 V, (E) −0.1 V and (G) −0.3 V with a constant charge of 0.2 C. (B), (D), (F) and (H) high magnification images corresponding to (A), (C), (E) and (G) respectively. Insets in the (B), (D), (F) and (H) represented the results of the contact angle measurements.

This surface would provide more interspaces for trapping of the air, and finally contributes to the large contact angle (Zhang et al., 2004, 2008; Chu et al., 2012). Thus, −0.1 V should be chosen as the deposition potential for the sake of optimal hydrophilicity and active area of the biosensor interface.

Similarly, the deposition time was studied in the range of 2–15 min under the potential of −0.1 V. The corresponding CV and FESEM characterizations were shown in Figs. S2 and S3 (Supplementary materials). The R_f values of these GMNs electrodes calculated to be 1.2 (2 min), 2.3 (4 min), 3.9 (6 min), 5.4 (8 min),

7.8 (10 min) and 8.4 (15 min), respectively, according to the Randles–Sevcik equation. Considering θ of the GMNs with the largest area is 82.3° (Fig. S4, Supplementary materials), it is much larger than that of GMNs with 10 min (θ=52.2°). Then, the deposition time of 10 min should be selected as the most suitable parameter.

Furthermore, the strong elemental gold peaks in the EDX spectrum of some HAG particles in Fig. 2E indicated gold was the only component of the obtained HAG (Supplementary materials, Fig. S5A). XPS is also an effective method to investigate the elemental composition of materials. Fig. S5B (Supplementary materials) showed the XPS spectrum of the HAG particles on the ITO surfaces. The gold $4f_{7/2}$ and $4f_{5/2}$ doublet with the binding energies of 84.2 and 87.9 eV indicated the gold valence state is in Au^0 (Cheng et al., 2003; Xu et al., 2010).

3.2. HAG enhanced DNA biosensors

The obtained HAG in this work possesses two merits. On the one hand, its large specific surface area and easy wettability are critical for DNA assay applications. On the other hand, previous studies proved that GMNs approximately separated at a distance of its radius could be acted as the microelectrodes (Karyakin et al., 2007; Cheng et al., 2002; Chu et al., 2011). In this case, the sensitivity and the signal-to-noise ratio of the DNA biosensors based on such HAG could be improved because of the enhanced diffusion profiles. Therefore, as a model, a "sandwich-type" DNA biosensor was fabricated. The fabrication procedure was shown in Fig. 3. Firstly, rDNA was chemi-absorbed to GNPs via a 3′ terminal thiol and then double stranded DNA functionalized GNPs (dsDNA–GNPs) were obtained by hybridization of rDNA with its partially complementary tDNA. The cDNA was immobilized onto the surface of the HAG electrode via the thiol–gold interaction. The other complementary part of tDNA could hybridize with the cDNA, so the dsDNA–GNPs could be immobilized on the electrode surface. The positive MB ions, which can bind to the anionic phosphate of DNA through electrostatic interaction at a low ionic strength (Ho et al., 1987), served as electrochemical probes here.

In contrast, in the absence of tDNA, the sandwich complex could not be formed, leaving the surface-confined cDNA unhybridized. Then, less MB molecules could be adsorbed onto the electrode surface, leading to a weaker electrochemical signal. The interaction of MB with dsDNA is considered to play a major role for the increased current responses of dsDNA than that of ssDNA (Kelley et al., 1997; Li et al., 2007). Also, more binding amount of MB by an electrostatic interaction at the dsDNA chain than that at ssDNA may contribute to the increased current responses of dsDNA.

3.3. The sensitivity of the HAG based DNA biosensor

Square wave voltammotric (SWV) measurements, which were found to provide excellent resolution of the electrochemical signal responses, were used to evaluate the performance of the DNA biosensor based on the HAG. As shown in Fig. 4A, a peak current of MB of 0.067 μA was obtained at the cDNA modified HAG electrode (curve a), which can be regarded as a blank signal (i_0). An increase (Δi_p) of about 0.083 μA in the SWV signal was observed after hybridization with fully complementary tDNA of 10 fM (curve b). Furthermore, it could be seen from Fig. 4B that the SWV peak current of MB on the HAG electrode increases with the increasing tDNA concentration. In Fig. 4C, the Δi_p of fabricated DNA sensor exhibited a linear correlation to the logarithm of the tDNA concentration ranged from 50 aM to 1 pM with linearity regression equation of Δi_p (μA)=0.064+0.031•log c (fM) (R^2=0.9986). According to the linear equation, we could detect tDNA concentration quantitatively. The detection limit was obtained as 12 aM (S/N=3), which is much lower or comparable with that of current many GMNs electrodes, listed in Table 1. Five independent electrodes were used simultaneously for the acquisition of each point in the calibration curve. The HAG with a huge surface area was considered to supply numerous attaching points for cDNA immobilization. And also, the immobilization orientation and

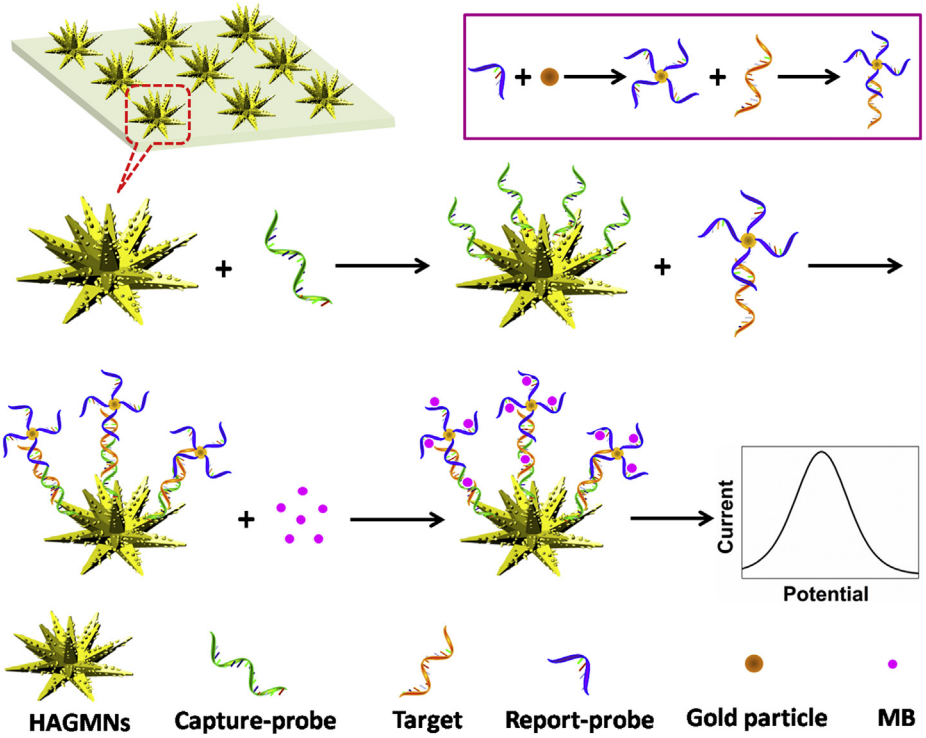

Fig. 3. Schematic illustration of the stepwise DNA sensor fabrication process.

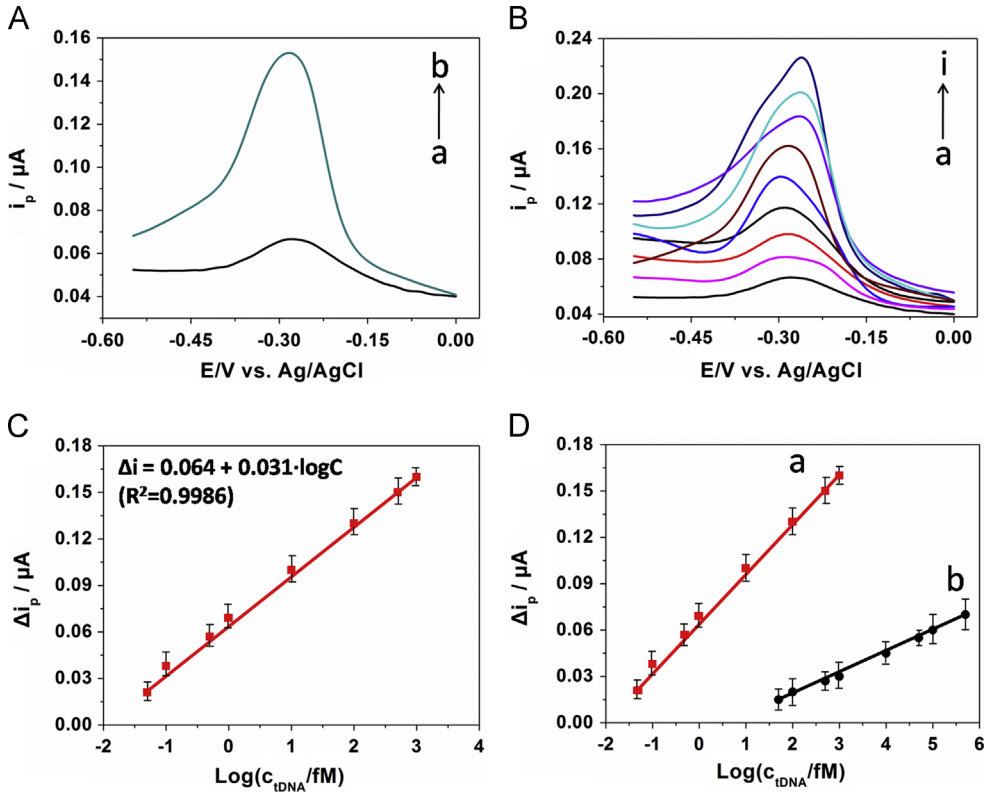

Fig. 4. (A) SWV responses of the cDNA-attached HAG electrode (a) before and (b) after the addition of 10 fM tDNA, (B) SWV responses of the cDNA-attached HAG electrode before and after the addition of different concentrations of tDNA strands, (a) blank solution, curves b to *i* represent 50 aM, 100 aM, 500 aM, 1 fM, 10 fM, 100 fM, 500 fM and 1 pM tDNAs, respectively. (C) Calibration curve for the DNA biosensor. (D) Calibration curves show Δi_p of different concentrations of tDNAs based on (a) HAG modified ITO electrode and (b) gold slice.

Table 1
Comparison of the assay performances of our DNA biosenor with those reported in the literatures.

GMNs	Detection limits	Linear detection range	Reference
HAG	12 aM	50 aM to 1 pM	This work
DenG	1 fM	1 fM to 1 nM	Li et al. (2011)
GNPs	1 pM	1 pM to 0.1 μM	L. Wang et al. (2011)
HHFG	19 fM	0.1 pM to 1 μM	X.X Wang et al. (2011)
GNPs	0.1 pM	–	Li et al. (2007)
GNPs	10 fM	50 fM to 10 pM	Zhang et al. (2006)
Hollow gold nanospheres	1 pM	1 pM to 10 nM	Liu et al. (2010)
GNPs	80 aM	0.1 fM to10 fM	Ren et al. (2010)
Gold nanowires	100 fM	–	Fang and Kelley (2009)
Nanoporous gold	28 aM	80 aM to 1.6 pM	Hu et al. (2008)

assembly density of cDNA may be well controlled by 3d dendritic structure of HAG for optimized hybridization efficiency. On the other side, the hierarchical 3d dendritic structure in present case may diminish the repelling behavior when approaching of the tDNA toward the immobilized cDNA and enhance the hybridization efficiency (Li et al., 2011).

Meanwhile, in the control experiment, DNA hybridizations based on the bare gold slice with the same geometrical area of 0.12 cm^2 were also investigated. Under the same condition during the process of probe immobilization and tDNA hybridization, a linear relation between the Δi_p and the logc (tDNA) was observed in a range from 50 fM to 500 pM, with detection limit of 20 fM (Fig. 4D). It should be noted that the DNA biosensor based on HAG possessed almost 3 orders of magnitude higher than that based on the bare gold slice.

3.4. The amplification of GNPs labels

Because GNPs serve a huge surface area, a single nanoparticle can be loaded with approximately one hundred DNA strands (Thaxton et al., 2005). The immobilization of dsDNA–GNPs complexes onto the electrode surface brought about the adsorption of large numbers of MB molecules, leading to an enhanced readout signal. For comparison, the SWV response of DNA biosensor without GNPs labels was also detected. As shown in Fig. 5A, after the tDNA with the concentration of 500 fM was introduced, the Δi_p of only 0.033 μA (curve b) was observed. While under the same condition, Δi_p of 0.126 μA (curve c) could be detected in the presence of the rDNA–GNPs.

3.5. Selectivity of fabricated DNA biosensor toward mismatched tDNA

The selective determination of current fabricated DNA biosensor toward one-base mismatched and full mismatched tDNA sequences has also been studied. As shown in Fig. 5B, the SWV peak current increase for one-base mismatched tDNA sequence was about 75% of that for perfectly matched tDNA of the same concentration (curve c). Whereas, almost the same peak current with the solely cDNA immobilized electrode was obtained when recognition with non-complementary tDNA (curve b). The SWV experiments showed a high selectivity of the constructed DNA biosensor for hybridization detection and the MB could be used as a good electrochemical indicator to properly discriminate the

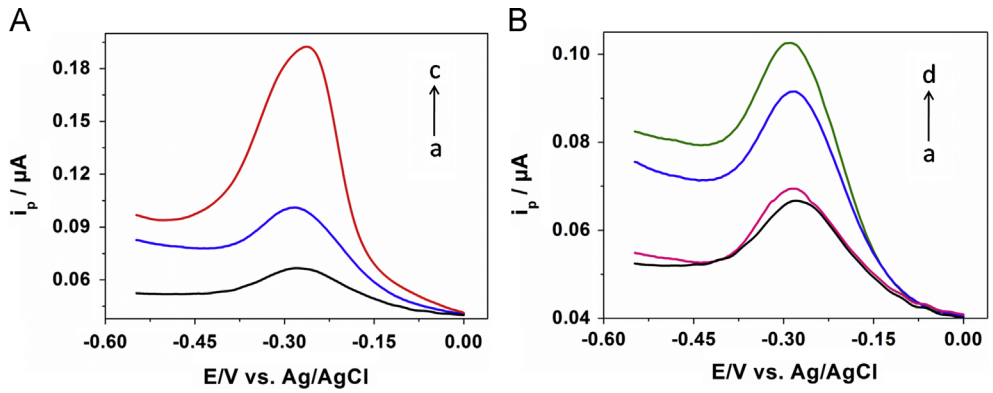

Fig. 5. (A) SWV responses of (a) cDNA only, (b) rDNA without GNPs labels and (c) in the presence of rDNA–GNPs. The added concentration of tDNA strands was 500 fM. (B) SWV responses of (a) cDNA only, (b) tDNA with full mismatched bases, (c) tDNA with single mismatched base, (d) complementary tDNA strands. The concentration of tDNA strands was 500 aM.

ssDNA and dsDNA by our fabricated strategy. It strongly indicated that the current fabricated DNA biosensor could be used to distinguish between complementary, non-complementary and mismatched DNA sequences.

3.6. *Regeneration and stability of the fabricated DNA biosensor*

The regeneration and stability of DNA biosensor is extremely important for the practical applications. It was found that the fabricated DNA biosensor could be regenerated 10 times with about 15% loss of the original signal by dipping the electrode in hot water (80 °C) for 15 min (Supplementary materials, Fig. S6A), followed by a rapid cooling in the ice bath for 10 min (Zhang et al., 2006; L. Wang et al., 2011). The signal attenuation may be due to the loss of probe strands on the HAG electrode surface. In addition, the probe modified electrode was firstly stored in the refrigerator at 4 °C for 1 week, 2 weeks and 3 weeks, respectively, and then examined after the hybridization with complementary tDNA strands. Experiments demonstrated that the DNA biosensor retained about 87% of its initial response even after 3 weeks (Supplementary materials, Fig. S6B).

4. Conclusions

A simple one-step electrodeposition method was used to fabricate HAG electrode. The electrodeposition of gold involved the formation of gold adatoms on both the ITO surface and gold nuclei, and gold aggregates increased their fractal dimension as the applied potential was shifted in the negative direction. Take into consideration of the surface wettability for fabricating an electrochemical DNA biosensor, the HAG with hydrophilic property as the building blocks could be obtained at −0.1 V for 10 min. The large surface area and specific 3d dendritic nanostructure of HAG were likely beneficial to increase the immobilization amount of cDNA. Furthermore, the GNPs labels could increase the immobilization amount of rDNA and then enhance the electrochemical readout signal. With the use of MB as an indicator, the optimized DNA biosensor could achieve a wide linear range from 50 aM to 1 pM for the tDNA detection with a detection limit of 12 aM. The current fabricated DNA biosensor should be also suitable for the detection of tDNA in real samples for clinical analysis. Moreover, the electrode modification strategy was expected for further extensive applications in other bioassays.

Acknowledgments

This work was supported by the National Natural Science Foundation of China (Nos. 21176115 and 20905035), Doctoral Fund of Ministry of Education of China (20113221110001), Innovation Foundation for Doctoral Dissertation of Jiangsu Province (CXLX12_0443) and State Key Laboratory of Materials-Oriented Chemical Engineering (KL10-15).

Appendix A. Supporting information

Supplementary data associated with this article can be found in the online version at http://dx.doi.org/10.1016/j.bios.2013.05.012.

References

Andreu, A., Merkert, J.W., Lecaros, L.A., Broglin, B.L., Brazell, J.T., El-Kouedi, M., 2006. Sensors and Actuators B 114, 1116–1120.
Brune, H., Roder, H., Bromann, K., Kern, K., Jacobsen, J., Stoltze, P., Jacobsen, K., Norskov, J., 1996. Surface Science 349, L115–L122.
Cao, Y., Searson, P.C., West, A.C., 2001. Journal of the Electrochemical Society 148, C376–C382.
Chen, X., Wang, Y., Zhou, J., Yan, W., Li, X., Zhu, J.J., 2008. Analytical Chemistry 80, 2133–2140.
Cheng, W.L., Dong, S.J., Wang, E.K., 2003. Langmuir 19, 9434–9439.
Cheng, W.L., Dong, S.J., Wang, E.K., 2002. Analytical Chemistry 74, 3599–3604.
Chu, Z., Shi, L., Zhang, Y., Jin, W., Xu, N., 2011. Journal of Materials Chemistry 21, 11968–11972.
Chu, Z., Shi, L., Liu, L., Liu, Y., Jin, W., 2012. Journal of Materials Chemistry 22, 21917–21922.
Daniel, M.C., Astruc, D., 2004. Chemical Reviews 104, 293–346.
Depestel, L.M., Strubbe, K., 2004. Journal of Electroanalytical Chemistry 572, 195–201.
Drummond, T.G., Hill, M.G., Barton, J.K., 2003. Nature Biotechnology 21, 1193–1199.
Fang, Z., Kelley, S.O., 2009. Analytical Chemistry 81, 612–617.
Finot, M.O., Braybrook, G.D., McDermott, M.T., 1999. Journal of Electroanalytical Chemistry 466, 234–241.
Gao, A.R., Lu, N., Dai, P.F., Li, T., Pei, H., Gao, X.L., Gong, Y.B., Wang, Y.L., Fan, C.H., 2011. Nano Letters 11, 3974–3978.
Giljohann, D.A., Seferos, D.S., Daniel, W.L., Matthew, M.D., Patel, P.C., Mirkin, C.A., 2010. Angewandte Chemie International Edition 49, 3280–3294.
Ho, P.S., Frederick, C.A., Saal, D., Wang, A.H., Rich, A., 1987. Journal of Biomolecular Structure and Dynamics 4, 521–534.
Hu, K., Lan, D., Li, X., Zhang, S., 2008. Analytical Chemistry 80, 9124–9130.
Ivanova, O.S., Zamborini, F.P., 2010. Analytical Chemistry 82, 5844–5850.
Jacobsen, J., Jacobsen, K.W., Stoltze, S., Norskov, J.K., 1995. Physical Review Letters 74, 2295–2298.
Jagerszki, G., Gyurcsanyi, R.E., Hofler, L., Pretsch, E., 2007. Nano Letters 7, 1609–1612.
Karyakin, A.A., Puganova, E.A., Bolshakov, I.A., Karyakina, E.E., 2007. Angewandte Chemie International Edition 46, 7678–7680.

Kelley, S.O., Barton, J.K., Jackson, N.M., Hill, M.G., 1997. Bioconjugate Chemistry 8, 31–37.
Lapierre-Devlin, M.A., Asher, C.L., Taft, B.J., Gasparac, R., Roberts, M.A., Kelley, S.O., 2005. Nano Letters 5, 1051–1055.
Li, D., Yan, Y., Wieckowska, A., Willner, I., 2007. Chemical Communications, 3544–3546.
Li, F., Han, X., Liu, S., 2011. Biosensors and Bioelectronics 26, 2619–2625.
Liu, J.W., Cao, Z.H., Lu, Y., 2009. Chemical Reviews 109, 1948–1998.
Liu, S., Liu, J., Han, X., Cui, Y., Wang, W., 2010. Biosensors and Bioelectronics 25, 1640–1645.
Ma, Z., Mao, Z., Gao, C., 2007. Colloids and Surfaces B 60, 137–157.
Martin, H., Carro, P., Creus, A.H., Gonzalez, S., Salvarezza, R.C., Arvia, A.J., 1997. Langmuir 13, 100–110.
Mazaira, D., Borras, C., Mostany, J., Scharifker, B.R., 2009. Journal of Electroanalytical Chemistry 631, 22–28.
Patolsky, F., Lichtenstein, A., Willner, I., 2003. Chemistry–A European Journal 9, 1137–1145.
Ren, R., Leng, C., Zhang, S., 2010. Biosensors and Bioelectronics 25, 2089–2094.
Saha, K., Agasti, S.S., Kim, C., Li, X., Rotello, V.M., 2012. Chemical Reviews 112, 2739–2779.
Sassolas, A., Leca-Bouvier, B.D., Blum, L.J., 2008. Chemical Reviews 108, 109–139.
Smilauer, P., Vvedenski, D.D., 1995. Physical Review B 52, 14263–14272.
Soleymani, L., Fang, Z.C., Sargent, E.H., Kelley, S.H., 2007. Nature Nanotechnology 4, 844–848.
Song, M.J., Kim, J.H., Lee, S.K., Lim, D.S., Hwang, S.W., Whang, D., 2011. Electroanalysis 23, 2408–2414.
Sun, Y.G., Xia, Y.N., 2004. Journal of the American Chemical Society 126, 3892–3901.
Thaxton, C.S., Hill, H.D., Georganopoulou, D.G., Stoeva, S.I., Mirkin, C.A., 2005. Analytical Chemistry 77, 8174–8178.
Wang, C.H., Yang, C., Song, Y.Y., Gao, W., Xia, X.H., 2005. Advanced Functional Materials 15, 1267–1275.
Wang, L., Chen, X., Wang, X., Han, X., Liu, S., Zhao, C., 2011. Biosensors and Bioelectronics 30, 151–157.
Wang, X.X., Yang, T., Li, X., Jiao, K., 2011. Biosensors and Bioelectronics 26, 2953–2959.
Xiao, L., Streeter, I., Wildgoose, G.G., Compton, R.G., 2008. Sensors and Actuators B 133, 118–127.
Xu, F., Cui, K., Sun, Y., Guo, C., Liu, Z., Zhang, Y., Shi, Y., Li, Z., 2010. Talanta 82, 1845–1852.
Zhang, C.Y., Yeh, H.C., Kuroki, M.T., Wang, T.H., 2005. Nature Materials 4, 826–831.
Zhang, H., Xu, J.J., Chen, H.Y., 2008. Journal of Physical Chemistry C 112, 13886–13892.
Zhang, J., Song, S., Wang, L., Pan, D., Fan, C., 2007. Nature Protocols 2, 2888–2895.
Zhang, J., Song, S., Zhang, L., Wang, L., Wu, H., Pan, D., Fan, C., 2006. Journal of the American Chemical Society 128, 8575–8580.
Zhang, X., Shi, F., Yu, X., Liu, H., Fu, Y., Wang, Z.Q., Jiang, L., Li, X.Y., 2004. Journal of the American Chemical Society 126, 3064–3065.
Zhang, Y., Cui, X., Shi, F., Deng, Y., 2012. Chemical Reviews 112, 2467–2505.